atmosphere

Article

Spatiotemporal Analysis of Hydrometeorological Factors in the Source Region of the Dongting Lake Basin, China

Shanshan Li [1,2], Changbo Jiang [1,3,*], Yuan Ma [1,3] and Chuannan Li [1,3]

1 School of Hydraulic Engineering, Changsha University of Science & Technology, Changsha 410114, China; ssli@stu.csust.edu.cn (S.L.); yma1@stu.csust.edu.cn (Y.M.)
2 College of Civil Engineering, Hunan City University, Yiyang 413002, China
3 Key Laboratory of Dongting Lake Aquatic Eco-Environmental Control and Restoration of Hunan Province, Changsha 410114, China
* Correspondence: jiangchb@csust.edu.cn; Tel.: +86-13875856755

Abstract: The Dongting Lake basin, located in the middle Yangtze River region, has long been under the threat of climate change. However, there has been a lack of comprehensive analysis and research on the long-term trends and interactions among hydrometeorological factors within the region. To address this gap, this study collected data from 31 meteorological stations in the region and employed statistical analysis methods, including the non-parametric Mann–Kendall test, Sen's slope test, and cross-wavelet analysis. The results revealed significant increases in temperatures, especially in the spring season, while summer, winter, and annual rainfall also exhibited a significant increase. However, spring and autumn rainfall showed a non-significant decrease, and there was a clear decreasing trend in annual streamflow. Interestingly, evaporation demonstrated a significant increasing trend. The annual average temperature and annual runoff exhibited approximately negative correlations in the 6–10-year resonance period and positive correlations in the 4–6-year resonance period. There are significant positive resonance periods in the relationship between annual precipitation and annual runoff within the range of 0–12 years, indicating that precipitation has a substantial impact and serves as the primary source of runoff. Furthermore, there was a transition between "abundance" and "dry" periods in the annual runoff around 4 a, occurring before and after 1973 and 2005. The change points in annual precipitation and runoff were identified as 1993 and 1983.

Keywords: spatiotemporal trend; hydroclimatic variables; the Dongting Lake basin

check for updates

Citation: Li, S.; Jiang, C.; Ma, Y.; Li, C. Spatiotemporal Analysis of Hydrometeorological Factors in the Source Region of the Dongting Lake Basin, China. *Atmosphere* **2023**, *14*, 1793. https://doi.org/10.3390/atmos14121793

Academic Editors: Davide Zanchettin and Tomeu Rigo

Received: 2 September 2023
Revised: 29 November 2023
Accepted: 30 November 2023
Published: 6 December 2023

1. Introduction

If global warming reaches 1.5 °C in the near future, it will further exacerbate the risks associated with climate disasters, posing multiple challenges to ecosystems and human well-being [1]. As global warming intensifies, the changes in regional temperature, rainfall, and evaporation become more pronounced [2]. By examining the hidden patterns within time series data of hydrometeorological variables such as temperature, rainfall, streamflow, and evaporation, we can gain insights into the overall changes and development trends over time [3]. This exploration is crucial for conducting scientifically informed hydrometeorological forecasting and effective water resource management. Moreover, the analysis of change points and trends in hydrometeorological variables has garnered increasing attention from scholars [4,5]. Human-induced climate change has had profound and wide-ranging impacts, leading to more frequent and intense extreme events that exceed the bounds of natural variability. These changes have caused significant losses and adverse effects on both ecosystems and human societies [6].

Changes in rainfall patterns, characterized by more intense but less frequent events, can contribute to increased drought severity within seasons, alter evapotranspiration rates, and generate changes in runoff [7]. The fact that rainfall occurrences resonate well with temperature changes in most areas of this region has led to an intensified hydrological cycle [8]. Therefore, it is essential to analyze the long-term trends of hydrometeorological variables and interactions among hydrometeorological factors. Such analyses enhance confidence in predicting future climate changes and have significant implications for water resource management [9]. Various methods are available for detecting trends in hydrometeorological variables. The non-parametric Mann–Kendall (MK) test is widely used to identify temporal trends in hydroclimatic time series [10–12]. To address serial autocorrelation issues in hydrometeorological data, Hamed and Rao [13] proposed an improved Modified MK test, which has been applied in numerous studies [14–17]. The Sen's slope (SS) test is another commonly used method for the trend analysis of hydrometeorological variables [18–20]. Change point analysis aims to identify significant breakpoints in time series, and the non-parametric Pettitt test has been widely utilized in the literature [21–23]. The Cross-Wavelet Transform is a novel multiscale analysis technique developed based on traditional wavelet analysis [24–26]. It not only efficiently analyzes the degree of correlation between two time series but also reflects their phase structure and fine features in both the time and frequency domains.

Dongting Lake, the second largest freshwater lake in China, is situated in the middle of the Yangtze River basin. The Dongting Lake basin, as a region with significant climate change within the Yangtze River basin, is also one of the most severely affected areas by flooding disasters [27]. The dynamic mechanisms linking climate warming and the exacerbation of floods, especially under the ongoing trend of rising temperatures, have become an urgent scientific issue that needs to be addressed. However, there are a limited number of studies on the trend analysis of various hydrometeorological parameters in the Dongting Lake basin.

Wang Guojie et al. [27] used the non-parametric Mann–Kendall (MK) test to analyze temperature, rainfall, and evapotranspiration trends in the Dongting Lake basin from 1960 to 2003. They found a significant warming trend in spring, autumn, and winter. They also noted increased annual rainfall and decreasing evapotranspiration. Xu Weihong et al. [28] employed the MK test and co-kriging interpolation to study rainfall variations from 1960 to 2011. They identified a decrease in annual rainfall, with changes in seasonal patterns. Li Jinggang [29] analyzed temperature changes in spring, autumn, and winter using meteorological statistics and GIS interpolation. The study showed significant warming in these seasons, particularly in spring. Zhang Meng et al. [30] examined surface evapotranspiration from 2000 to 2014 using MOD16 data. They discovered spatial variations and an overall decrease in average evapotranspiration.

These studies primarily focused on individual climatic factors, with some lacking periodic analysis. At the same time, the analysis of trends, abrupt changes, and periodicity in hydro-meteorological factors serves as a foundational step in constructing drought prediction models [31] and hydroclimate models [32]. The goal of this study is to investigate the spatiotemporal trends and abrupt changes in maximum, minimum, and mean temperatures, rainfall, evapotranspiration, and their potential relationships in the Dongting Lake basin, utilizing hydro-meteorological data spanning from 1960 to 2019.

2. Materials and Methods

2.1. Study Area

The Dongting Lake basin (24°35′–30°27′ N, 107°13′–114°18′ E) is the largest lake watershed in China, covering a total area of 26.3×10^4 km^2, accounting for 14.6% of the Yangtze River basin. The basin consists of sub-basins including the Dongting Lake area, Xiang River, Zi River, Yuan River, and Li River. It spans parts of Guizhou, Guangxi, Chongqing, Hubei, Jiangxi, and Guangdong provinces, as well as the entire province of Hunan. Hunan province alone covers 21.18×10^4 km^2, which accounts for 80.61% of the Dongting Lake basin area (Figure 1). The Dongting Lake basin has a complex and diverse topographic variety, with its eastern, western, and southern sides surrounded by mountains, whose elevations range from 19 to 2558 m. The Dongting Lake basin experiences a typical continental subtropical monsoon climate, hot and rainy summers, and dry and cool winters.

The climate exhibits significant interannual variations, with annual average temperatures ranging from 15 °C to 18 °C. Annual rainfall shows a substantial variation and uneven distribution, ranging from 1148 mm to 1837 mm [33]. In China, where the average annual precipitation is 630 mm, the Dongting Lake basin is considered to be an area with abundant rainfall. Figure 1 illustrates the study area, reservoirs, and selected meteorological stations utilized in this research.

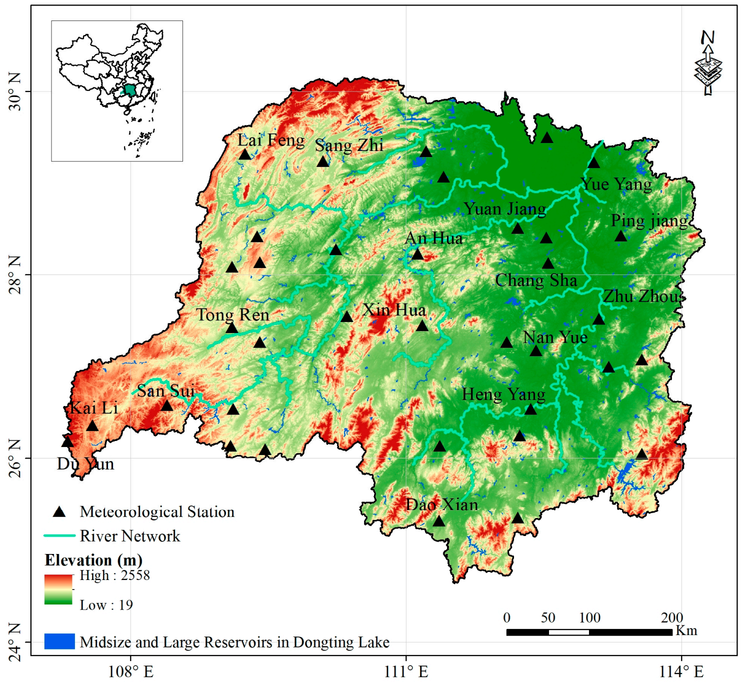

Figure 1. The hydrological and reservoir layout of the Dongting Lake basin.

2.2. Data Source and Processing

The data for maximum, average, and minimum temperatures, rainfall, and evaporation utilized in this study were obtained from the China Meteorological Science Data Sharing Service Network (http://data.cma.cn (accessed on 1 February 2021)). Quality control procedures were applied to all station data, including a manual review process in which station data with a missing rate exceeding 20% were excluded. South Yue Station is located at an elevation of 1268.5 m, significantly higher than the elevations of other surrounding meteorological stations. Due to its windward-slope topography, this station experiences orographic rainfall effects, resulting in an annual precipitation of 2051.3 mm, which significantly deviates from the annual precipitation observed at neighboring meteorological stations. As a result, data from this station were not included in the rainfall analysis. Additionally, the quality control process addressed the identification and handling of possible outliers. The streamflow data used in this study were acquired from the Chenglingji hydrological station, which serves as the outlet control station for the Dongting Lake basin. The hydrometeorological data cover the period from January 1960 to December 2019. The reservoir data were obtained from the study conducted by Song et al. [34] (https://essd.copernicus.org/articles/14/4017/2022/ (accessed on 1 February 2021)). Considering the climatic characteristics of the Dongting Lake basin, this study defined four seasons: spring (March to May, SP), summer (June to September, SU), autumn (October to November, AU), and winter (December of the current year to February of the following year, WI).

2.3. Methods

2.3.1. Non-Parametric Mann–Kendall (MK) Test

We used the non-parametric time series trend test proposed by Mann–Kendall [35,36] to detect potential trends in the century-long precipitation series. The MK trend test requires the assumption of a null hypothesis (assuming that the sequence has no significant trend) and an alternative hypothesis (assuming that the sequence has a significant upward or downward trend). The statistical test statistic s and its variance var(s) in the MK trend test are calculated using the following formulas:

$$S = \sum_{i=1}^{n=1} \sum_{t=i+1}^{n} G(\phi) \tag{1}$$

$$G(\phi) = \operatorname{sgn}(x_t - x_i) = \begin{cases} 1 & (x_t - x_i) > 0 \\ 0 & (x_t - x_i) = 0 \\ -1 & (x_t - x_i) < 0 \end{cases} \tag{2}$$

$$\operatorname{var}(s) = \frac{\left[n(n-1)(2n+5) - \sum_{i=1}^{m} r_i(r_i - 1)(2r_i + 5)\right]}{18} \tag{3}$$

In the equation, x represents the time series variable; n is the number of variables in the sequence; $\operatorname{sgn}(x_t - x_i)$ is the sign function; m represents the number of repeated data groups in the sequence; and r_i represents the number of repeated data in the i-th group.

To perform a significance test, the statistic is standardized. The formula for the statistic Z is as follows:

$$Z = \begin{cases} \frac{S-1}{\sqrt{\operatorname{var}(S)}} & S > 0 \\ 0 & S = 0 \\ \frac{S+1}{\sqrt{\operatorname{var}(S)}} & S < 0 \end{cases} \tag{4}$$

At a given significance level, α = 0.05; if $|Z| > Z_{1-\alpha/2}$, the null hypothesis is rejected. This indicates the presence of a significant upward trend. If the test statistic S is less than the negative of the critical value $-Z\alpha/2$, the null hypothesis is rejected, indicating a significant downward trend. Conversely, if the test statistic S falls within the range between $-Z\alpha/2$ and $Z\alpha/2$, the null hypothesis is accepted.

2.3.2. Modified Mann–Kendall (MMK) Test

MMK is a method proposed by Hamed and Rao (1998) to address the issue of serial correlation in time series data. They suggested using a variance correction method to improve trend analysis. By incorporating lagged values into the function, considering significant lags up to the nth lag, the accuracy of trend detection is further enhanced [13].

MMK primarily focuses on modifying the variance formula in order to replace the original variance in MK. It aims to correct the errors caused by autocorrelation between the observed data. The modified variance formula, denoted as var(s)*, is calculated as follows:

$$\operatorname{var}(s)^* = \operatorname{var}(s)\left[1 + \frac{2}{n(n-1)(n-2)} \sum_{i=1}^{n-1} (n-i)(n-i-1)(n-i-2)W_S(i)\right] \tag{5}$$

$$W_S(i) = \frac{n \sum_{j-1}^{n-1} (x_j - \overline{x})(x_{j+1} - \overline{x})}{(n-i) \sum_{j=1}^{n} (x_j - \overline{x})^2} \tag{6}$$

In the equation, n represents the number of observed values, and $W_s(i)$ represents the autocorrelation function of the observed sequence.

In this study, a significance level of α = 0.05 is chosen, which means that $Z_{1-\alpha/2} = 1.96$, and when $|Z| > 1.96$, the sequence exhibits a significant upward or downward trend. Conversely, there is no significant trend [13].

2.3.3. Non-Parametric Pettitt Test

Pettitt [37] proposed a non-parametric approach to identify change points in a time series. It is a rank-based, distribution-free test which detects a significant change in the mean of a time series. Similar to the MK method, a rank sequence is constructed following Equation (1). However, there are three different definitions for m_i, depending on the three cases:

$$m_i = \begin{cases} +1 & x_i > x_j \\ 0 & x_i = x_j \\ -1 & x_i < x_j \end{cases} \qquad j = 1, 2, \ldots, i \tag{7}$$

In the given context, the rank sequence d_k represents the cumulative count of instances where the value at time i is greater or less than the value at time j. The Pettitt method directly utilizes the rank sequence to detect change points. If the time t_0 satisfies the condition

$$kt_0 = Max|d_k| \quad k = 2, 3, 4, \ldots, n \tag{8}$$

then the mutation point is at point t_0.

$$P = 2\exp\left(\frac{-6K_{t_0}^2}{n^3 + n^2}\right) \tag{9}$$

When $P \leq 0.5$, then the detected mutation point is considered statistically significant. In addition, sequential versions of the MK test statistic [38,39] have been used to validate the change points obtained using the Pettitt test.

2.3.4. Sen's Slope (SS) Test

Sen's slope estimator is a non-parametric method proposed and developed by Sen [40] in 1968 for estimating the trend slope of N pairs of data out of n samples.

$$\mathrm{Q_i} = \frac{x_j - x_k}{j - k} \qquad (\mathrm{i} = 1, 2, \ldots, N) \tag{10}$$

In the equation, x_j and x_k represent the time series values of the jth and kth samples, respectively ($j > k$). If there is only one observation in each time period, then $N = \frac{n(n-1)}{2}$, where n is the number of time periods. However, if there are multiple observations within one or more time periods, then $N < \frac{n(n-1)}{2}$.

Arranging the N $\mathrm{Q_i}$ values in ascending order, the median of Sen's slope estimates can be calculated as follows:

$$\mathrm{Q_{med}} = \begin{cases} Q[(N+1)/2] & N \textit{ is odd} \\ \frac{Q[N/2] + Q[(N+1)/2]}{2} & N \textit{ is even} \end{cases} \tag{11}$$

The sign of Q_{med} reflects the direction of the data trend, while the magnitude of Q reflects the magnitude of the trend.

2.3.5. Wavelet Analysis

Air temperature, precipitation, and discharge time-series are rarely stationary and they consist of a broad set of transient patterns varying within the temporal record. The wavelet transform allows the transient patterns recorded in such non-stationary time-series to be localized in both time and periodicity. It thus provides a complete time-scale representation of localized and transient phenomena occurring at different time-scales [41]. In this research, we make use of the Morlet wavelet, which was successfully used in the past to analyze precipitation, temperature, and discharge time-series [42–44].

(1) The Continuous Wavelet Transform (CWT)

The CWT [45] is based on the concept of wavelets, which are localized oscillatory functions that are well-suited for capturing localized features in a signal. The transform involves convolving the signal with a family of scaled and translated wavelet functions, known as the analyzing wavelet. These wavelet functions are generated by dilating and translating a mother wavelet function.

Mathematically, the Continuous Wavelet Transform of a signal $x(t)$ with respect to a wavelet function $\psi(a,b)$ is given by the following integral:

$$CWT(a,b) = \frac{1}{\sqrt{a}} \int x(t)^* \psi^*(t-b)dt \tag{12}$$

where * denotes the complex conjugate, a represents the scale parameter that controls the dilation of the wavelet function, b represents the translation parameter that shifts the wavelet function along the time axis, and $\psi^*(t-b)$ is the complex conjugate of the wavelet function.

The resulting CWT coefficients represent the strength and phase information of the signal at different scales and positions in time. By varying the scale and position parameters, the CWT provides a time–frequency representation of the signal, revealing how the frequency content of the signal evolves over time.

(2) The Cross-Wavelet Transform (XWT)

XWT [24] combines the concepts of wavelet transform and cross-spectral analysis, allowing for the exploration of the correlation between two time series in both the time and frequency domains. Assuming that $W_n^X(s)$ and $W_n^Y(s)$ represent the Continuous-Wavelet Transform (CWT) of two time series $X = \{x_1, x_1, \cdots, x_n\}$ and $Y = \{y_1, y_1, \cdots, y_n\}$, the Cross-Wavelet Transform between them is given by $W_n^{XY}(s) = W_n^X(s)W_n^{Y*}(s)$. $W_n^{Y*}(s)$ represents the complex conjugate of $W_n^Y(s)$, and "s" represents the time lag (also known as the time shift). The cross-wavelet power spectrum can be defined as $\left|W_n^{XY}(s)\right|$, the following field containing time–frequency–amplitude information, and a higher value indicates a higher level of correlation between the two time-series. For two stationary random processes, the normalized form of the XWT can be written as the wavelet cross-correlation coefficient:

$$\mathrm{r}(X,Y) = \frac{\sum_{i=1}^{n} (W_i^X(s) - \overline{W_i^X(s)})(W_i^Y(s) - \overline{W_i^Y(s)})}{\sqrt{\sum_{i=1}^{n} (W_i^X(s) - \overline{W_i^X(s)})^2}\sqrt{\sum_{i=1}^{n} (W_i^Y(s) - \overline{W_i^Y(s)})^2}} \tag{13}$$

Another quantity used to reflect the degree of coherence between two wavelet transforms in the time–frequency domain is the Wavelet Coherence (WTC). In this study, the Morlet wavelet is chosen as the wavelet basis function to reflect the time–frequency structural characteristics of the correlation oscillations between the two time-series after undergoing wavelet transformation in both the time and frequency domains.

2.3.6. Method of Spatial Interpolation

Spatial interpolation was employed to estimate values at unsampled locations based on the observed data points. Kriging, a geostatistical interpolation technique, which estimates values in unknown regions by considering both the distance and degree of variation between known data points [46]. Kriging considers not only the spatial autocorrelation but also the variance between data points, providing more accurate predictions.

The Kriging process involves creating a mathematical model that characterizes the spatial correlation structure of the variable under consideration. In our study, Kriging was applied to generate spatial fields for the variables of interest, including temperature, rainfall, and evapotranspiration.

This interpolation method is advantageous as it considers both the spatial trends and the uncertainty associated with the predictions, offering a robust spatial estimation technique.

3. Results and Analysis

3.1. Temperature

Figure 2 illustrates the spatial variation in annual temperature parameters, including daily maximum (Tmax), average (Tmean), and minimum (Tmin) temperatures, across the Dongting Lake basin from 1960 to 2019. The data reveal notable distinctions in temperature distributions within the basin. Tmax displays a clear gradient pattern, with the highest values recorded at the Daoxian meteorological station in Hunan and the lowest at the Sansui meteorological station in the mountainous area of Guizhou. As we move from the peripheral hills towards the interior plains, Tmax gradually increases, while it decreases with increasing latitude. Tmin exhibits a similar trend to Tmax, reflecting lower temperatures in the eastern, western, and northern regions, while the southern region experiences the highest Tmin values, consistent with Tmean. In terms of Tmean, higher temperatures are observed in the southern region with lower latitudes and the central–northern plains. These temperature patterns gradually decrease from the southeast to the northwest, with the southern region having temperatures around 17–18 °C and the northwestern areas in Xiangxi recording temperatures below 16.5 °C.

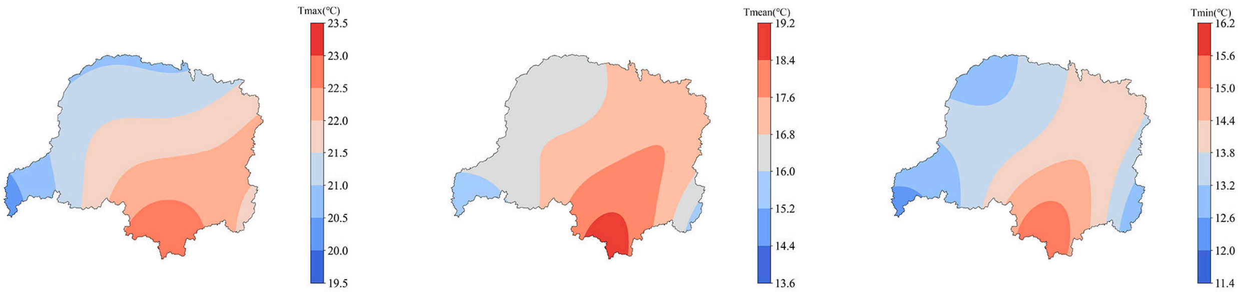

Figure 2. The spatial distribution of annual average maximum, average, and minimum temperatures in the Dongting Lake basin.

The results of the non-parametric MK test (for serially independent series), the MMK test (for serially correlated series), and the SS test (trend magnitude) applied to monthly, annual, and seasonal time-series for various temperature datasets are presented in Figures 3–5. Figure 3 illustrates that the Tmax time-series during spring exhibits a significant increasing trend, indicating a warming trend in spring temperatures. Moreover, the Tmax time series for January displayed a decreasing trend, while increasing trends were observed for the other months. Regarding the Tmean time series, excluding the summer season, a significant increasing trend was observed in the spring, autumn, winter, and annual time-series. Specifically, the average temperature exhibited the most significant increase in March, April, and October (Figure 4). However, the Tmean time series for August displayed a decreasing trend, while the other months showed increasing trends. In Figure 5, the Tmin time series showed a significant decreasing trend in July and August, resulting in a negative trend for Tmin during the summer season. Overall, the Tmax monthly, annual, and seasonal time-series indicated an increasing trend, while the Tmin monthly, annual, and seasonal time-series displayed a decreasing trend at two grid points.

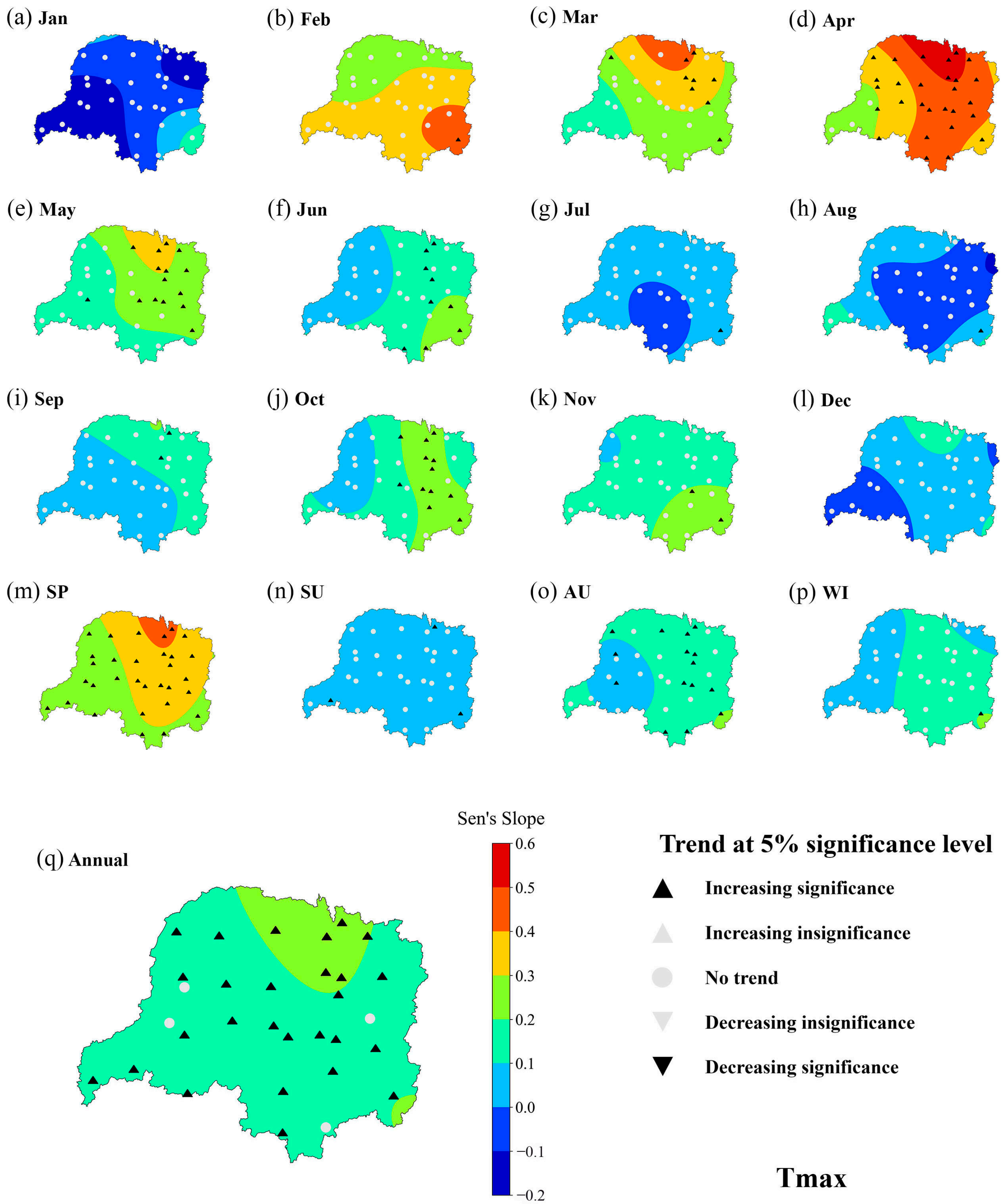

Figure 3. The spatial variation trends and Sen's slopes of the monthly, seasonal, and annual Tmax time-series in the Dongting Lake basin. The units for Sen's slope are as follows: monthly trend (°C/month), quarterly trend (°C/quarter), and annual trend (°C/year).

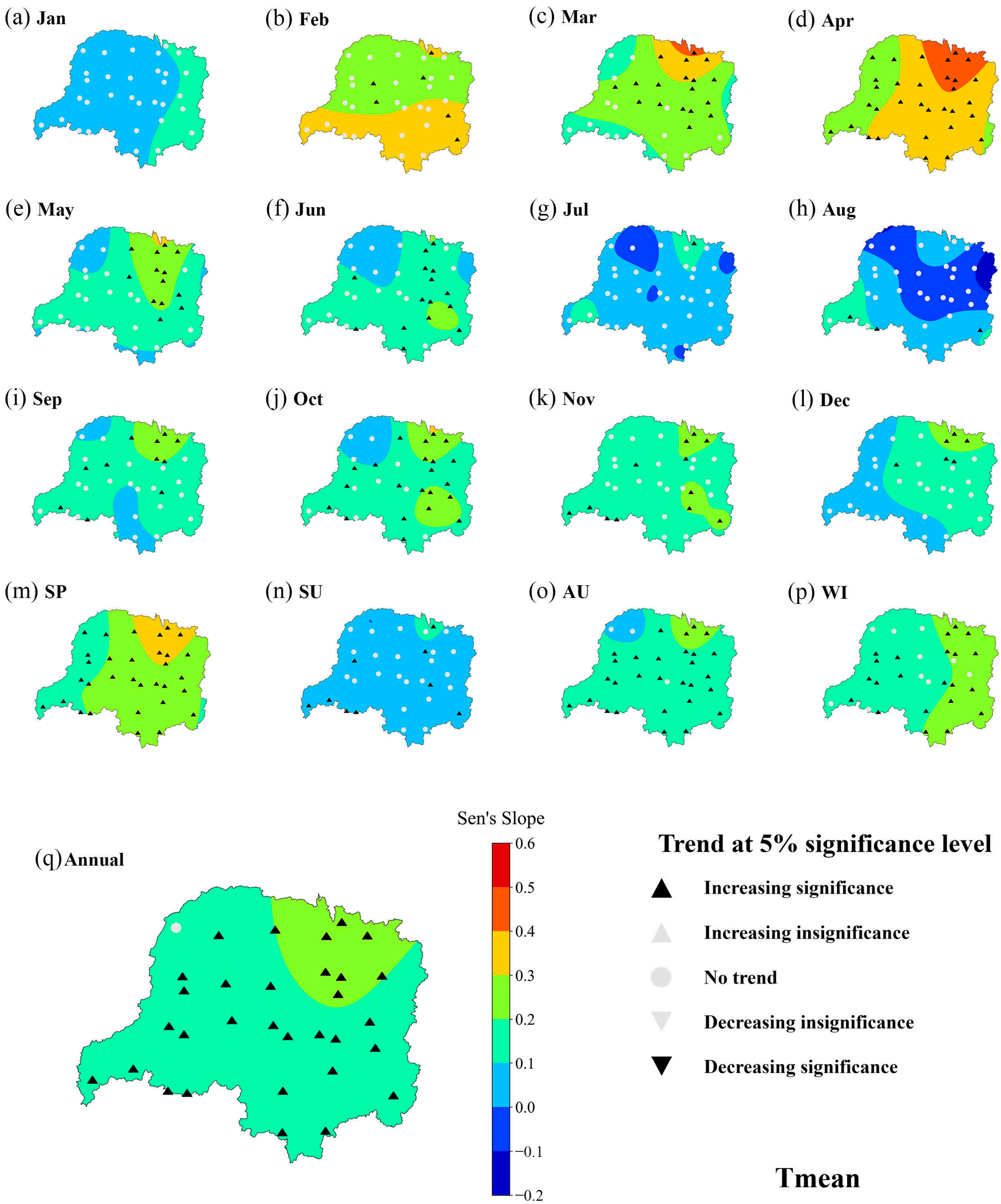

Figure 4. Same as Figure 3 but for Tmean time series.

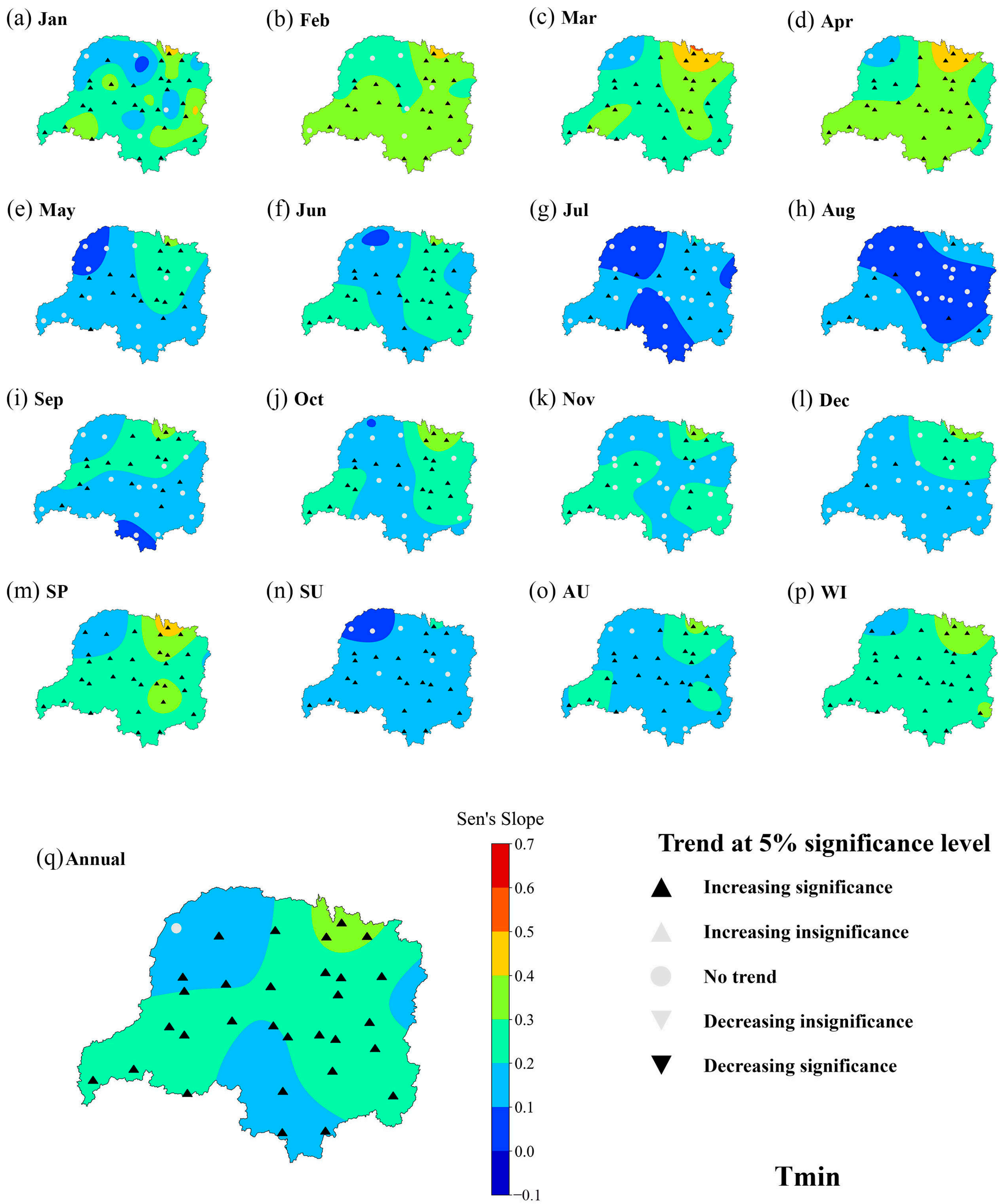

Figure 5. Same as Figure 3 but for Tmin time series.

Figures 3–5 also present the slope values indicating the magnitude of trends for the monthly, seasonal, and annual time series of Tmax, Tmean, and Tmin at the meteorological stations. The average Tmax, Tmean, and Tmin time series in the basin exhibited increasing trends in both the seasonal and annual data. Among them, the spring season displayed the highest growth rate, with Tmax, Tmean, and Tmin increasing at rates of 0.312 °C, 0.252 °C, and 0.27 °C per quarter, respectively. On the other hand, the summer season had the lowest growth rate, with Tmax, Tmean, and Tmin increasing at rates of 0.042 °C, 0.06 °C, and 0.138 °C per quarter, respectively. From the graphs, it can be observed that Tmin showed more increasing trends compared with Tmax and Tmean, except in the spring season. Overall, the annual time series for Tmax, Tmean, and Tmin exhibited growth rates of 0.168 °C, 0.18 °C, and 0.222 °C per year, respectively. All temperature time series demonstrated slightly higher growth rates in the spring and winter seasons, with the Tmin time series in winter showing a more pronounced increasing trend. The values obtained from the SS test complemented the trend characteristics observed from the MK test results in different time series.

3.2. Rainfall

The spatial distribution of annual rainfall in the Dongting Lake Basin is depicted in Figure 6. The central, southern, and eastern regions of the basin experience relatively abundant rainfall, while the western regions receive less precipitation. There is a gradual decrease in rainfall from the southeast to the northwest. Areas such as Anhua, Pingjiang, and Zhuzhou receive higher annual rainfall, averaging over 1500 mm. The primary sources of water for the Dongting Lake basin are the regions located at the eastern and western ends of the Pacific Equator, the eastern Pacific Ocean, and the northern part of the Indian Ocean. As a result of monsoonal storms predominantly impacting the southern and southeastern parts of the catchment area, the southern region receives higher rainfall. Moreover, the hilly terrain at the southern edge of the basin acts as a barrier, hindering the moisture-laden winds flowing from the southeast to the north. Therefore, the annual precipitation in the southern region of the catchment area averages over 1500 mm, while in the western region, the annual precipitation is at its lowest, below 1200 mm.

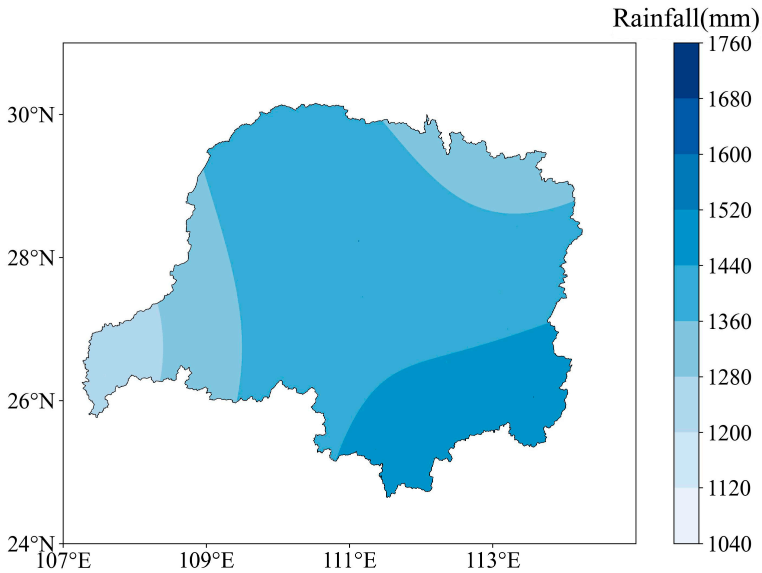

Figure 6. The spatial distribution of annual rainfall in the Dongting Lake basin.

The study first conducted tests to examine the existence of sequential correlation among various rainfall time series from 30 meteorological stations within the basin and the average basin rainfall values. Subsequently, non-parametric MK tests (for serially independent series), MMK tests (for serially correlated series), and SS tests (for trend magnitude) were applied to the monthly, annual, and seasonal time-series of various temperature datasets based on the test results, as shown in Figure 7. The results indicate that significant sequential correlation is only present in the annual time series at the Yuanling weather station, while monthly, seasonal, and annual time-series at all other weather stations do not exhibit significant sequential correlation. The trend analysis reveals that in April, 12 out of the 30 meteorological stations display a significant decreasing trend in their time series (Figure 7d). Additionally, in October, four meteorological stations show a pronounced decreasing trend in rainfall time series (Figure 7j). On the other hand, the time series for January, March, June, and July display sporadic increasing trends at scattered grid points, with significant summer trends observed in the central region and significant winter trends in the northeastern region at a 5% level of significance.

During spring and autumn, a majority of the meteorological stations exhibited a decreasing trend in rainfall time series (Figure 7m,o). Specifically, the decreasing trend in spring was observed in the central and western regions, while in autumn, it was prevalent in all regions except for certain parts of the north. The analysis of temperature trends suggests that the decreasing temperature trend in July and August may enhance the process of cloud condensation in the region, leading to a significant increase in summer rainfall. Conversely, the warming trend in spring may weaken the condensation of moisture in the air, resulting in a decreasing trend in spring rainfall. However, it is important to note that the performance of regional-scale rainfall is influenced by various factors at both regional and global scales, including aerosols, greenhouse gas concentrations, land cover changes, and ENSO (El Niño–Southern Oscillation), among others.

In general, the trend analysis of annual total rainfall in the region indicates an increasing trend over time. However, there are specific seasonal variations observed. The trend analysis results reveal a decreasing trend and drier conditions in the spring and autumn seasons. The southern part of the basin receives the highest rainfall, with an increasing trend in annual rainfall. On the other hand, the western part of the region exhibits relatively lower rainfall and shows a further decreasing trend in annual rainfall. Figure 7 also provides the results of the SS test, which show the trend magnitudes of monthly, annual, and seasonal rainfall time series for the 30 grid points. From the figure, it can be observed that the trend magnitudes of the December time series are nearly zero for all the grids and the basin average. The analysis further indicates that the summer, winter, and annual average rainfall in the Dongting Lake basin are increasing at rates of 31.2 mm, 4.2 mm, and 10.2 mm per quarter, respectively. On the other hand, the rainfall in spring and autumn shows a decreasing trend of 7.8 mm and 3 mm per quarter, respectively. Overall, the results obtained from the SS test are consistent with the findings of the MK test, providing further support for the observed rainfall trends in the region.

In addition to analyzing the temporal trends of rainfall time series, the study also investigated the occurrence of change points in the annual time series spanning from 1960 to 2019. Table 1 summarizes the change points in the annual rainfall series obtained through the Pettitt test for each meteorological station. The table presents the year of the change point, its corresponding p-value, and the change in the average annual value following the change point. Among the 30 meteorological stations, the majority of change points were observed around 1989 and 1993. In 1993, a change in the annual average rainfall was observed for the entire basin based on calculations using the Thiessen polygon method with data from the 30 meteorological stations. Figure 8 provides an illustration of the evaluation of the annual average rainfall time series in the basin, utilizing the Pettitt test statistic and the plot of the series values against time for the MK test statistic. While the Pettitt test statistic reaches its maximum value in 1993, indicating a change point, the plot of the MK test statistic displays a pattern of continuous increases and decreases. Nevertheless, the MK-Z value continues to rise after 1993, confirming the change point identified by the Pettitt test. Hence, it can be confidently stated that 1993 marks the change point for annual rainfall in the Dongting Lake basin. Furthermore, with the exception of seven meteorological stations, the annual rainfall at the remaining twenty-three stations exhibits a positive shift. Figure 9 visualizes the changes in the annual rainfall time series before and after the identified change point. It reveals an increase from 1376.8 mm before the change to 1437.3 mm after the change, indicating a rise of 60.5 mm since 1993. This increase accounts for approximately 4% of the pre-change average annual rainfall, signifying a relatively modest change.

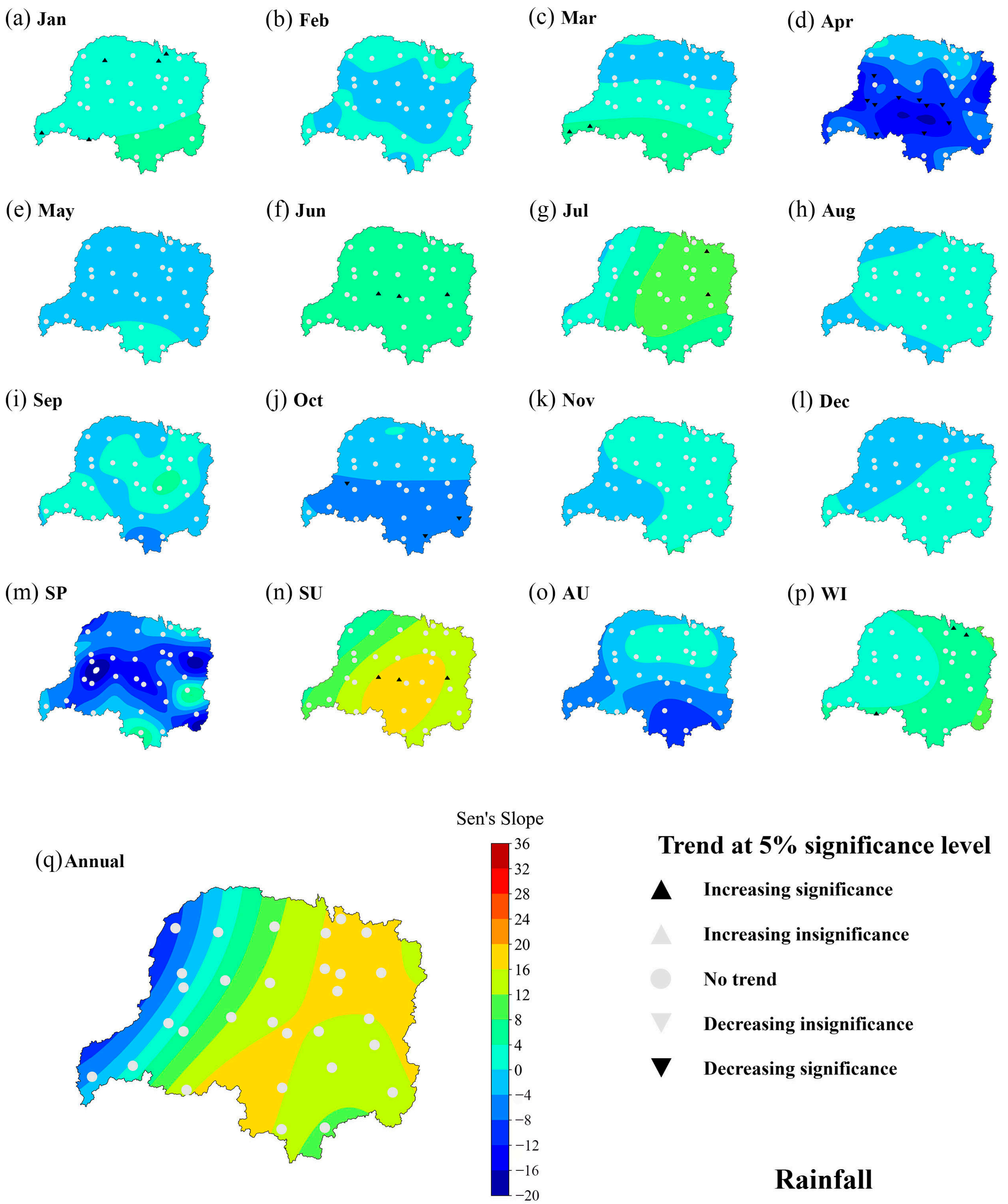

Figure 7. The spatial variation trends and Sen's slopes of the monthly, seasonal, and annual rainfall time-series in the Dongting Lake basin. The units for Sen's slope are as follows: monthly trend (mm/month), quarterly trend (mm/quarter), and annual trend (mm/year).

Table 1. Summary of Pettitt test results for annual rainfall at meteorological stations.

Stations	*n*	*p*-Value	Year	Variation
LaiFeng	60	0.516	24	−98.3
Sangzhi	60	0.979	33	55.9
Shimen	60	0.804	52	126.8
Jianli	60	0.336	20	131.7
Nanxian	60	0.638	27	60.2
Yueyang	60	0.211	27	144.4
Baojing	60	0.734	18	−90.8
Jishou	60	0.495	52	223
Yuanling	60	0.715	50	140.3
Anhua	60	0.423	29	105.9
Yuanjiang	60	0.686	29	68.7
Xiangyin	60	0.722	29	96.3
Changsha	60	0.103	29	119.9
Pingjiang	60	0.46	43	−106.9
Tongren	60	0.842	52	133.3
Zhijiang	60	0.551	13	−116.5
Xupu	60	0.523	30	91
Xinhua	60	0.092	29	135
Shaoyang	60	0.828	28	57.5
Shuangfeng	60	0.34	27	68.2
Youxian	60	0.576	20	124.7
Zhuzhou	60	0.114	30	142.5
Kaili	60	0.794	18	−62.3
Sansui	60	0.558	23	−68
Tongdao	60	0.336	8	239.5
Yongzhou	60	0.658	52	159.1
Hengyang	60	0.774	47	−114.5
Guidong	60	0.223	33	140.3
Daoxian	60	0.466	52	319.3
Jiahe	60	0.842	33	64.5

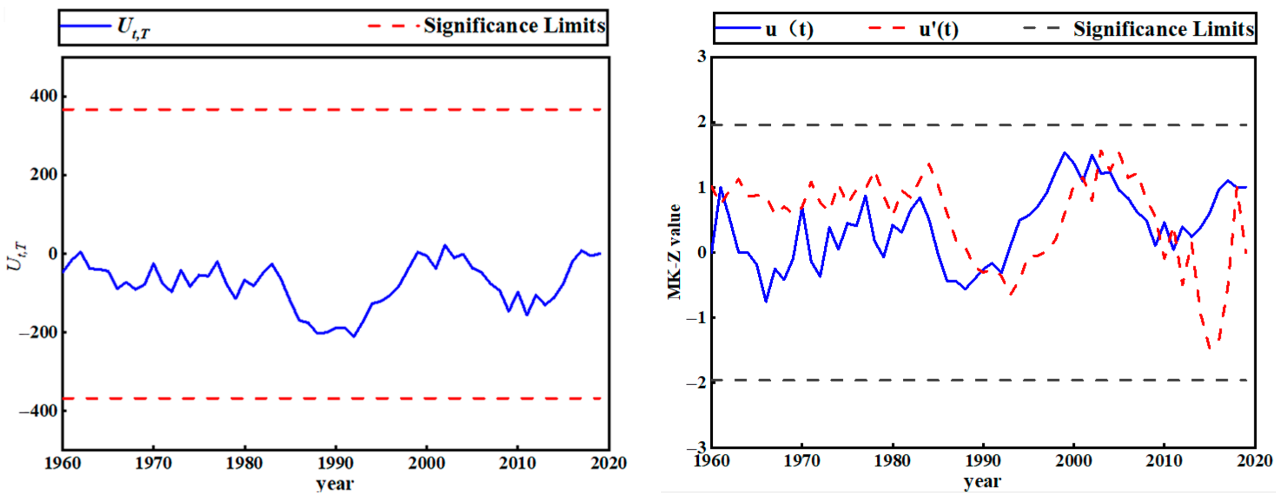

Figure 8. The Pettitt test statistic (**left**) and the MK-Z values of the sequence (**right**) for the non-significant change point in the annual average rainfall in the Dongting Lake basin in 1993.

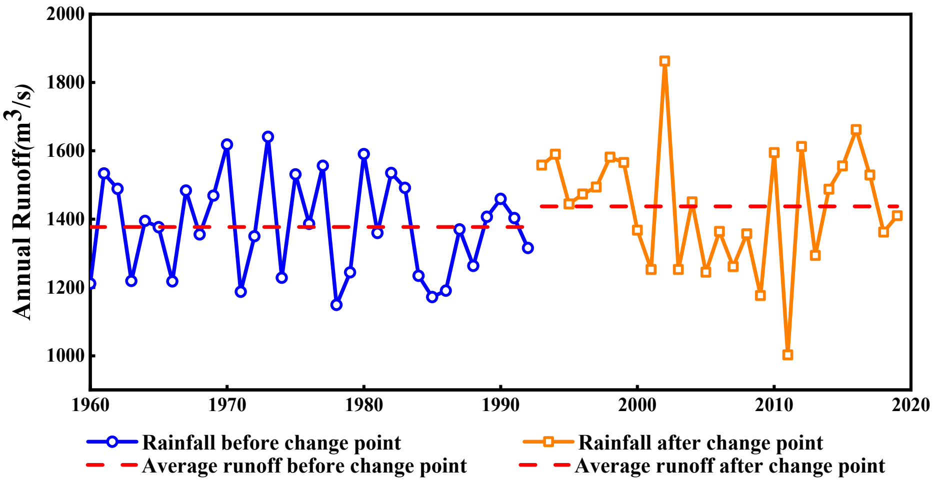

Figure 9. Time series plot of annual rainfall in the Dongting Lake basin, indicating a positive transfer mutation in 1993.

3.3. Runoff

During the period spanning from 1960 to 2019, the annual runoff in the Dongting Lake basin, measured at the Chenglingji hydrological station at the basin's outlet, exhibited a range of variability between 1475.4 and 4007.9 $\times$ 10^8 m^3. Based on the results of the autocorrelation test presented in Table 2, significant serial correlations were found in the October and autumn runoff time series. Specifically, the runoff time series for January, February, and winter exhibit significant increasing trends at a 5% significance level, while the other months, seasons, and the annual time-series show decreasing trends. The results of the SS test in Table 2 indicate a significant decreasing trend in the annual runoff time series, with a decrease rate of 11,573 m^3 per year. The spring, summer, and autumn runoff sequences also show decreasing trends at rates of 1544.7 m^3, 5436.5 m^3, and 7971.1 m^3 per year, respectively, while the winter runoff sequence displays an increasing trend at a rate of 1287 m^3 per year. Overall, a decreasing trend is observed in most of the runoff in the Dongting Lake basin, highlighting the need for careful planning and efficient water resource systems in the region.

Table 2. Results of series correlation, MK, MMK, SS, and Pettitt tests at Chenglingji hydrographic station, 1960–2019.

Time Series	Correlation	MK/MMK Test (Z)	SS Test (β)	*p*-Value	Year	Shift
Jan	independent	3.31	756.8	0.003	9	+
Feb	independent	2.4	596.8	0.023	9	+
Mar	independent	1.89	1013.4	0.051	0	+
Apr	independent	−1.32	−870.1	0.382	9	-
May	independent	−1.82	−1711.6	0.01	8	-
Jun	independent	−0.47	−428.9	0.544	5	-
Jul	independent	−1.78	−2525.2	0.134	0	-
Aug	independent	−2.21	−2303.7	0.065	0	-
Sep	independent	−3.62	−3616.1	0.012	0	-
Oct	correlation	−5.59	−3279	0	0	-
Nov	independent	−2.61	−1378.5	0.026	4	-
Dec	independent	−0.39	−103.4	0.243	1	-
Spring	independent	−0.99	−1544.7	0.402	8	+
Summer	independent	−2.24	−5436.5	0.099	0	-
Autumn	correlation	−4.81	−7971.1	0	0	-
Winter	independent	2.15	1287.3	0.013	9	-
Annual	independent	−2.54	−11,573.7	0.023	4	-

Table 2 presents the results of the Pettitt test, and Figure 10 displays the test statistic plot. The analysis reveals a significant change in annual runoff occurring in 1983, as evidenced by the observed change point being statistically significant at the 5% level with a p-value of 0.023, which is lower than 0.05. The results of the consecutive MK test further support the identification of the change point established by the Pettitt test. Figure 11 illustrates the MK-Z values, illustrating the variations in annual runoff over the specified period. It is noticeable that the annual runoff displayed an increasing trend prior to 1983, followed by a decreasing trend until approximately 1990, with a slight increase in the subsequent decade and a sharp decline from 2003 to 2019. Hence, it is justifiable to consider 1983 as the change point for the annual runoff at the Chenglingji hydrological station in the Dongting Lake basin. The annual runoff time series at the basin outlet experienced a decrease in 1983, and the average annual runoff decreased by 376.7 × 108 m^3 after the change point (Figure 11).

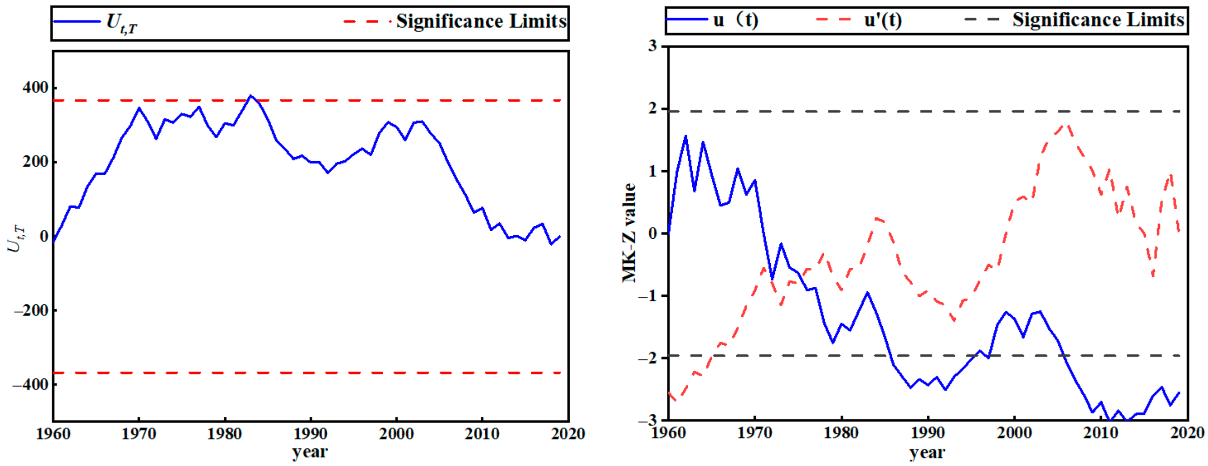

Figure 10. Pettitt's test statistic (**left**) and serial MK-Z values (**right**) of runoff from Chenglingji hydrological station at the non-significant variation point in 1983.

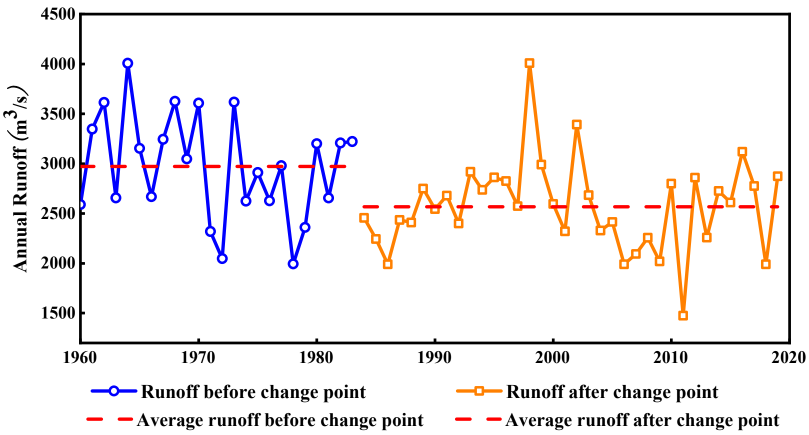

Figure 11. Time series plot of runoff from Chenglingji hydrological station, indicating a positive transfer mutation in 1983.

3.4. Evapotranspiration

Evaporation, as a key element in the water cycle, plays a crucial role in hydrological and meteorological processes. In the Dongting Lake basin, the results of autocorrelation tests on monthly, seasonal, and annual time-series of evaporation from 31 meteorological stations indicate that there is significant serial correlation in the average series for the northern region in the months of January, February, March, April, May, and November, while the southern region shows a significant serial correlation only in July. Based on the results of serial correlation, MK (or MMK) and SS tests were conducted, as shown in Figure 12.

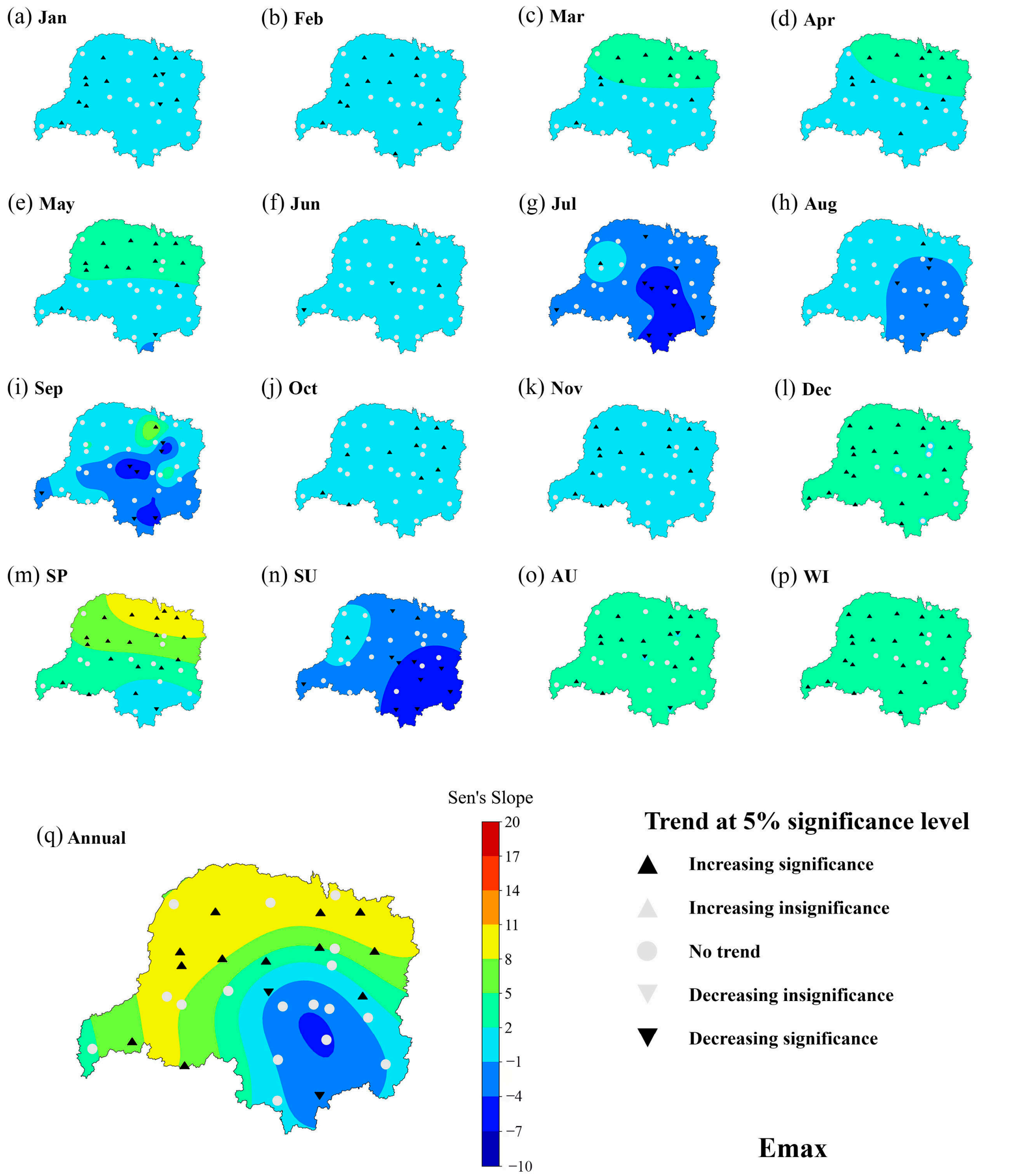

Figure 12. Spatial trends and SS of monthly, quarterly, and annual evapotranspiration time-series in the Dongting Lake basin. The units for Sen's slope are as follows: monthly trend (mm/month), quarterly trend (mm/quarter), and annual trend (mm/year).

From the figure, it can be observed that there are significant increasing trends in the ET (evapotranspiration) time-series during the spring and winter seasons. Furthermore, a significant increasing trend in annual ET was observed at 12 meteorological stations in the northern part of the Dongting Lake basin. As shown in Figure 12, the SS test results indicate increasing trends in ET for the spring, autumn, winter, and annual time-series in the basin, with growth rates of 5.11 mm, 2.22 mm, 4.66 mm per quarter, and 4.44 mm per year, respectively. However, there is a decreasing trend in summer, with a reduction rate of 2.91 mm.

3.5. Cross-Wavelet Analysis of Rainfall, Temperature, and Runoff

The Morlet wavelet function was employed to perform wavelet transforms on the annual rainfall, annual average temperature, and annual runoff in the Dongting Lake basin. The continuous wavelet spectra of these variables from 1960 to 2019 were obtained and are visualized in Figure 13. In the figure, the red and blue colors represent the peaks and valleys of the energy density, respectively, reflecting the local and dynamic characteristics of the time–frequency transformation of the dominant wavelet components. The darkness or lightness of the colors indicates the relative changes in energy density. The thick solid black line represents the 95% confidence interval boundary, indicating that it has passed the red noise test. The thin solid black line represents the wavelet cone of influence boundary, which denotes the areas more affected by the edge effects of the continuous wavelet transform data [24].

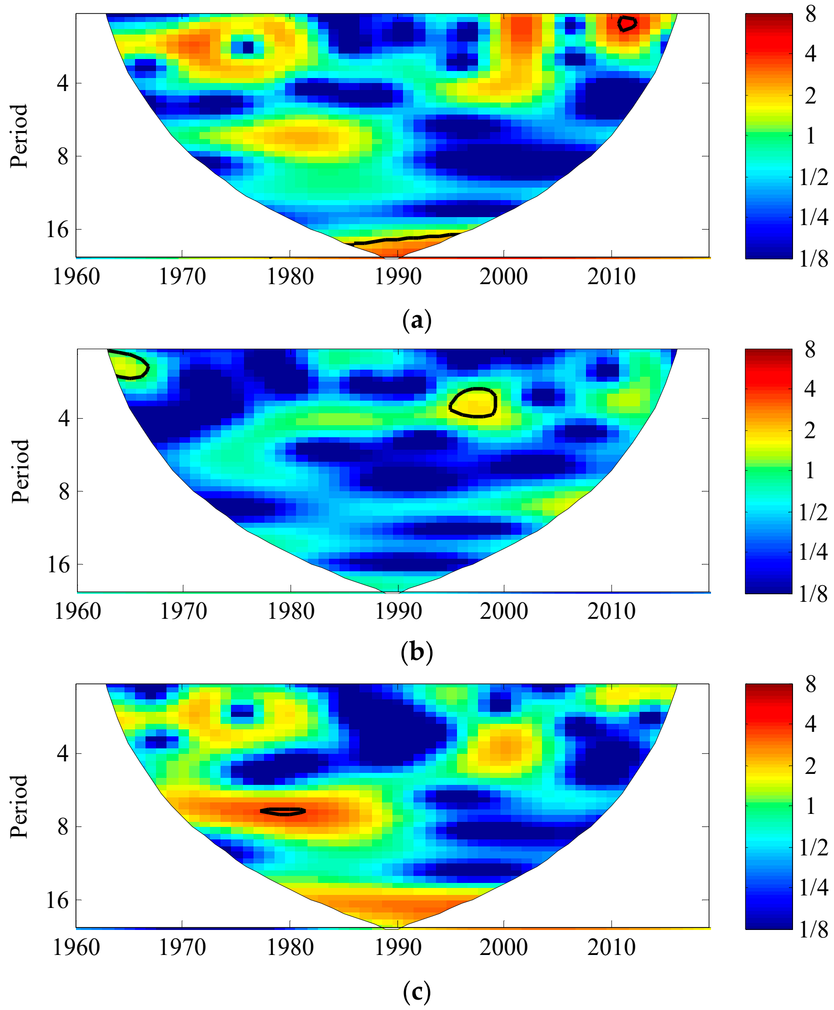

Figure 13. Continuous wavelet analysis of rainfall (**a**), temperature (**b**), and runoff (**c**).

Continuous wavelet analysis was employed to investigate the periodicity of annual rainfall, annual mean temperature, and annual runoff in the Dongting Lake basin. Figure 13a reveals that the annual rainfall in the basin exhibits one cycle, with a period of approximately 1 year around 2010. Figure 13b indicates that the annual mean temperature demonstrates two cycles: a cycle of around 1–2 a from 1961 to 1970 and another cycle of approximately 3–4 a from 1994 to 2000. Figure 13c shows that the annual runoff at the Chenglingji hydrological station displays a single cycle, with a period of approximately 7a around 1980. It is worth noting that the periodicity of annual rainfall and annual runoff in the Dongting Lake basin exhibit similarity, with the cycle of annual runoff occurring roughly 30 a earlier than that of annual rainfall.

By employing cross-wavelet transform and wavelet coherence analysis on the coefficients derived from the continuous wavelet transform of rainfall, temperature, and annual runoff in the Dongting Lake basin, the wavelet coherence spectra between these variables were examined. The significance of the coherence spectra was evaluated using the standard spectra, enabling the exploration of their correlation in the time–frequency domain across various time scales [47]. The results are illustrated in Figure 14. In Figure 14, the direction of the arrows indicates the phase relationship between rainfall and runoff, as well as temperature and runoff. Arrows pointing from left to right (→) indicate that the variables change in the same phase and exhibit a positive correlation. Arrows pointing from right to left (←) indicate an anti-phase relationship and a negative correlation. Arrows pointing vertically downward (↓) and upward (↑) represent the wavelet transform of rainfall and temperature leading and lagging runoff by a quarter of a 20-period cycle, demonstrating a nonlinear correlation [48]. The region encompassed by the fine arcs in the figure corresponds to significant spectral values.

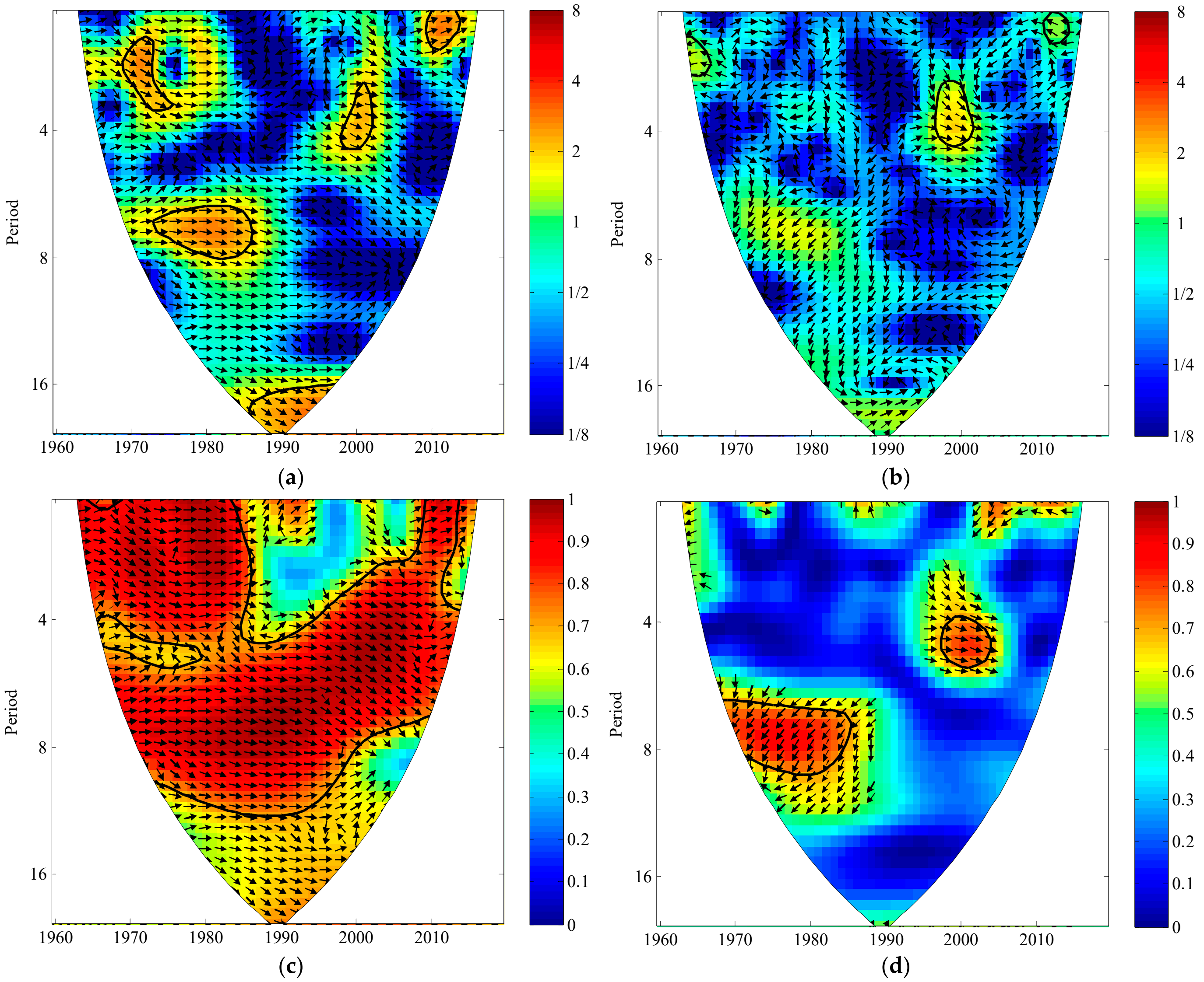

Figure 14. Cross-wavelet transform and wavelet coherence between the Dongting Lake basin annual rainfall and annual runoff (**a**,**c**), and average temperature and annual runoff (**b**,**d**).

Figure 14a,c displays the cross-wavelet power spectrum and wavelet coherence spectrum between annual precipitation in the Dongting Lake basin and annual discharge at the Chenglingji station. From the cross-wavelet energy spectrum in Figure 14a, two significant features are observed: ① A period of 6–8 years (1973–1986), demonstrating a strong positive correlation with high energy concentrated mainly around the 7a cycle in the mid-to-high-frequency range, gradually transitioning from low to high frequencies. ② Resonance periods of 1–2a (2008–2012), 2–4a (1968–1975), and 3–5a (1998–2002), characterized by relatively small regions in the confidence test, indicating intermittent quasi-periodic oscillations. The cross-wavelet coherence spectrum in Figure 14c reveals a strong positive correlation. The regions that pass the significance test account for more than 90% of the entire wavelet cone of influence. In the high-frequency region with a 3a cycle, a mutation in the resonance period occurred around 1988 and the years around 2005.

The annual precipitation in the Dongting Lake basin exhibits a very strong positive correlation with the annual discharge at the Chenglingji station. More than 90% of the entire wavelet cone of influence passed the significance test, indicating a significant relationship between the basin's precipitation and discharge. This suggests that precipitation plays a substantial role in supplying the basin's discharge. In the high-frequency region with a 4a cycle, a resonance period mutation occurred around 1973 and the years around 2005, signifying a transition between "abundance" and "dry" periods in the Dongting Lake basin during that time frame.

Figure 14b,d illustrates the cross-wavelet power spectrum and wavelet coherence spectrum between the annual average temperature in the Dongting Lake basin and the annual discharge at the Chenglingji station. From the cross-wavelet energy spectrum in Figure 14b, two significant features pass the 90% confidence test: ① Periods of approximately 1–2a (around 1965–1969 and between 1977–1993), with phase angles showing a nearly positive correlation. ② A period of 3–5a (1996–2001), exhibiting an approximately positive correlation with a phase angle. The relationship experienced a phase transition around 1990 and the years around 2005. In the earlier time domain, before 1990, there was a negative correlation between discharge and temperature changes, while after 1990, a positive correlation emerged. In the later time domain, the phase angles were relatively chaotic. The cross-wavelet coherence spectrum in Figure 14d shows a negative correlation within the 6–10a scale (1968–1986) and a positive correlation within the 4–6a scale (1996–2004). The distributions of high energy and phase angle direction are very close, indicating intermittent quasi-periodic oscillations.

The response of annual mean discharge to changes in annual mean temperature is negatively correlated, indicating that a short-term increase in temperature leads to increased evaporation within the basin, subsequently reducing the contribution to river discharge. Conversely, the annual mean temperature is positively correlated with the annual mean discharge, suggesting that warming intensifies snow and ice melt, thereby increasing the contribution to river discharge.

4. Discussion

The objective of this study was to assess the spatial and temporal patterns, as well as the cyclic variations, in the monthly, seasonal, and annual time series of maximum, minimum, and average temperatures, rainfall, runoff, and evapotranspiration in the Dongting Lake basin. The temperature trends observed at the watershed scale are not consistent with the results of studies conducted by some scholars at the watershed scale. In Zhou Hui's study [49] on the temperature in the Dongting Lake basin from 1960 to 2013, it was indicated that the average temperatures in spring, summer, autumn, and winter exhibited a gradual upward trend, with the most significant temperature increase observed in winter. However, this current study reveals that the highest increase in Tmean is observed in spring, emphasizing a notable warm spring phenomenon, while the warming trend in summer within the basin is not significant. The magnitude of temperature increase shows inconsistency with Zhou Hui's research but generally aligns with the findings of Li

Jinggang et al. [29]. However, neither of these studies considered the changing trends in T_{max} and T_{min} time series.

Inconsistent trends were observed in rainfall patterns across different seasons, with a majority of meteorological stations showing a decreasing trend in spring and autumn rainfall, while summer and winter rainfall exhibited an increasing trend. It is worth noting that the rainfall trends in winter, spring, and autumn are synchronous with the runoff trends, while the rainfall trends in summer are opposite to the concurrent runoff trends. This aligns with the findings of Xu Weihong et al. [28] regarding annual rainfall in the Dongting Lake basin from 1960 to 2011.

Given the significant influence of the Asian monsoon climate, summer rainfall contributes substantially to the total annual rainfall in the Dongting Lake Basin. The increasing trend in summer rainfall suggests an adequate amount of rainfall during the wet season. On the other hand, the decreasing trend in spring and autumn rainfall indicates drier conditions during the dry seasons, which can lead to a significant freshwater shortage in the region. This highlights the importance of effective water resource management strategies during the dry seasons. However, when examining the runoff trends, a consistent decline was observed across all seasons. The interannual variability of annual runoff in Dongting Lake is influenced by a combination of factors, including climate change and human activities. Climate change can bring about alterations in hydrological conditions at the basin outlet through changes in rainfall patterns, evaporation rates, temperature fluctuations, and other related factors. Simultaneously, human activities, such as the construction of dams, reservoir operations, landscape reconstruction, and channel excavation, also play a role in impacting the variability in annual runoff. These complex factors interact and contribute to the observed changes in annual runoff in the Dongting Lake basin [50].

4.1. Sen's Slope Spatial Variability Analysis

The Sen's slope within the watershed exhibits spatial variation, despite the relatively small size of the watershed. This spatial variability may be influenced by a variety of factors. A number of studies [51,52] have explored the effects of topography and elevation differences on temperature variations within watersheds. Variances in topography and altitude within the watershed may lead to temperature variations across different regions. Higher-altitude areas generally tend to exhibit lower temperatures, whereas lower-altitude regions might experience higher temperatures. The terrain of the Dongting Lake basin is complex and diverse, surrounded by mountains in the east, west, and south, with altitudes ranging from 19 to 2588 m; in the central part, the terrain is hilly and basin-like, with altitudes ranging from 50 to 400 m; and in the northern part, the terrain is a plain, forming a unique horseshoe shape, with altitudes ranging from 25 to 40 m [53].

Different land use and land cover types, such as forests, agricultural fields, urban areas, etc., can significantly impact local temperatures [54]. For instance, urban areas often experience the urban heat island effect, leading to higher temperatures within cities. Over the past 60 years, land use in the Dongting Lake Basin has changed dramatically. The presence of water bodies within the watershed (such as lakes, rivers, etc.) can also influence temperature distribution [54]. Water bodies can absorb and release heat, creating distinct temperature patterns around aquatic environments. Cheng Gong's study found a negative correlation between Hovenia dulcis and air temperature in Dongting Lake Basin [55].

Considering these factors holistically, the diverse spatial pattern of Sen's slope within the watershed is reasonable. Future research could delve deeper into analyzing the interactions among these factors to gain a more comprehensive understanding of the mechanisms underlying temperature variations.

4.2. Impact of Reservoir Construction

Climate change has had a notable impact on runoff patterns in the Dongting Lake basin. While climate change has generally led to an increase in rainfall, human activities have contributed to a decrease in runoff, resulting in an overall declining trend. Specifically, summer rainfall has increased, and there is a less pronounced warming trend in the region. Evapotranspiration, which refers to the combined process of water evaporation from the land surface and transpiration from plants, has decreased over time. This decrease in evapotranspiration, coupled with the declining trend in runoff, may be attributed to human activities. Human-induced changes that affect runoff can be categorized into direct impacts, such as the construction of reservoirs, and indirect impacts, such as changes in land use and land cover that alter the conditions for runoff generation. As of 2020, the Dongting Lake basin is home to a considerable number of reservoirs, including 56 large-scale reservoirs with a total capacity of 421.58 $\times$ 10^8 m^3 and 388 medium-sized reservoirs with a total capacity of 106.31 $\times$ 10^8 m^3. The trends in rainfall and runoff show a distinct contrast. Despite the positive trend in rainfall, there has been a negative trend in the runoff. The turning point for increased annual rainfall occurred in 1993, while the turning point for decreased runoff occurred in 1983. From 1985 to 1990, there was a significant increase in water storage in the reservoirs within the Dongting Lake basin [56]. It is important to note that the influence of land use and land cover changes on runoff is primarily limited to the non-monsoon seasons, highlighting the complex interplay between climate change, human activities, and the hydrological dynamics of the region. Further research and analysis are necessary to better understand the specific mechanisms and interactions driving these trends in the Dongting Lake basin, which will contribute to improved water resource management and sustainable development in the area.

Dam construction plays a significant role in altering the runoff patterns within the Dongting Lake basin. This human activity, which involves the construction of reservoirs, has resulted in a decrease in runoff despite an increasing trend in rainfall. Figure 15 demonstrates a notable increase in the total water storage capacity of reservoirs within the basin over the study period. It is worth noting that the inflection points observed in the rainfall trend do not align with those observed in the runoff. This indicates that human activities, such as dam construction, play a dominant role in shaping the temporal patterns of annual runoff. However, to gain a comprehensive understanding, further research is necessary to investigate the underlying mechanisms through which these human activities impact lake runoff. Additionally, it is important to assess the individual contributions of different factors to the overall changes in runoff within the basin. By conducting detailed studies and analyses, researchers can shed more light on the specific ways in which human activities, including dam construction, influence runoff dynamics in the Dongting Lake basin. This knowledge will be invaluable for effective water resource management and sustainable development in the region.

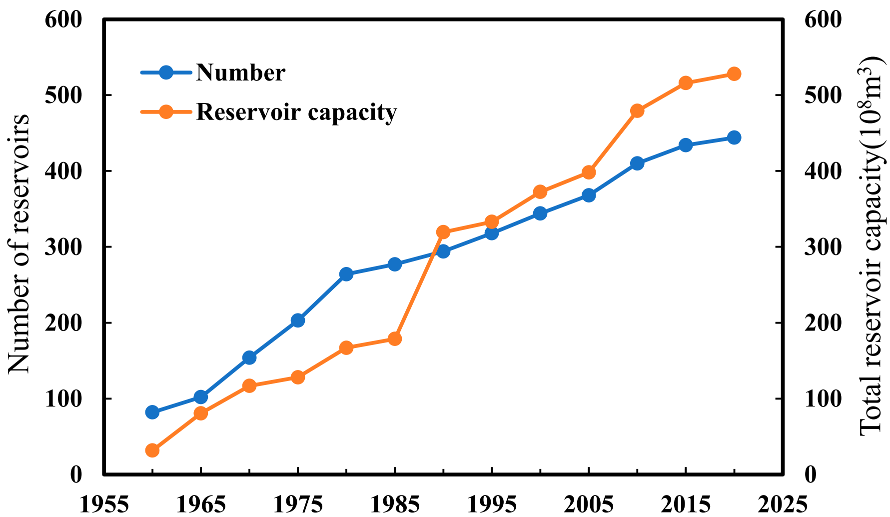

Figure 15. Analysis of the number and total capacity of large- and medium-sized reservoirs in the Dongting Lake basin.

5. Conclusions

The trend and change point analysis was carried out for thirty-one meteorological stations and one hydrometric station in the Dongting Lake basin over different time periods. The cross-wavelet transform was used to analyze the correlation between the measured annual runoff at Chenglingji Hydrological Station and the two influencing factors, and to reveal the degree of correlation and detailed characteristics at different time and frequency scales. The main observed findings of the current work can be summarized as follows:

(1) During the study period, the minimum, maximum, and average temperatures showed an overall increasing trend, with spring temperatures having a significant upward trend. The annual time series for Tmax, Tmean, and Tmin exhibited growth rates of 0.168 °C, 0.18 °C, and 0.222 °C per year, respectively.

(2) The annual total precipitation in the Dongting Lake basin exhibits a year-by-year increasing trend at a rate of 10.2 mm per year, while the precipitation during the spring and autumn seasons shows a decreasing trend at rates of 7.8 mm and 3 mm per year. The annual runoff at the basin outlet exhibits a clear decreasing trend at rate of 11,573 m^3 per year. Furthermore, the long-term time series of evaporation also shows an increasing trend at rates of 4.44 mm per year. The change points identified using the non-parametric Pettitt test for annual rainfall and annual runoff were inconsistent, occurring in 1993 and 1983, respectively.

(3) The annual average temperature and annual runoff in the Dongting Lake basin show a negative correlation cycle of 6–10a. As the temperature increases, evaporation in the basin increases, leading to a decrease in runoff. There is also a positive correlation cycle of 4–6a, where spring warming intensifies glacier melting, resulting in increased water supply to the rivers. The annual rainfall and annual runoff exhibit a good positive correlation cycle of 0–12a, indicating that rainfall is a controlling factor for runoff and is the main source of water supply in the Dongting Lake basin. In the high-frequency region with a 3a cycle, a mutation in the resonance period occurred around 1973 and the years around 2005.

The variation in runoff in the Dongting Lake basin is the result of the combined effects of climate change and human activities. Quantitative investigations on the impacts of climate change and human activities on water flow will require the integration of hydrological models for analysis. This will be explored in future research.

Author Contributions: C.J. edited the manuscript and contributed as a supervisor; S.L. designed the framework of this study and was responsible for writing—original draft preparation and analysis; Y.M. wrote some codes for data processing; and C.L. helped with the drawing. All authors discussed the results and implications of the manuscript at all stages. All authors have read and agreed to the published version of the manuscript.

Funding: This research was funded by the National Natural Science Foundation of China (No. 52109006) and the Research Foundation of Education Bureau of Hunan Province, China (No. 22B0305).

Institutional Review Board Statement: Not applicable.

Informed Consent Statement: Not applicable.

Data Availability Statement: The following supporting information can be downloaded online: http://www.gscloud.cn (accessed on 15 August 2023), geographical information: The Geospatial Data Cloud for the SRTMDEMUTM 90 m product; http://data.cma.cn (accessed on 15 August 2023), ground observation datasets: Precipitation at 31 stations downloaded from the Nation Meteorological Information Center. The reservoir data were obtained from https://essd.copernicus.org/articles/14/4017/2022/ (accessed on 15 August 2023).

Acknowledgments: We acknowledge the hydrometeorological factors data from the National Meteorological Information Center. The authors also gratefully acknowledge Yizhuang Liu for helping with the publication.

Conflicts of Interest: The authors declare no conflict of interest in the publication of this paper.

References

1. Intergovernmental Panel on Climate Change (IPCC). *Climate Change 2022: Impacts, Adaptation and Vulnerability. Contribution of Working Group II to the Sixth Assessment Report of the Intergovernmental Panel on Climate Change*; Cambridge University Press: Cambridge, UK, 2022.
2. McCrystall, M.R.; Stroeve, J.; Serreze, M.; Forbes, B.C.; Screen, J.A. New climate models reveal faster and larger increases in Arctic precipitation than previously projected. *Nat. Commun.* **2021**, *12*, 6765. [CrossRef]
3. Li, C.; Liu, Z.; Li, W.; Lin, Y.; Hou, L.; Niu, S.; Xing, Y.; Huang, J.; Chen, Y.; Zhang, S. Projecting future risk of dengue related to hydrometeorological conditions in mainland China under climate change scenarios: A modelling study. *Lancet Planet. Health* **2023**, *7*, e397–e406. [CrossRef] [PubMed]
4. Fooladi, M.; Golmohammadi, M.H.; Safavi, H.R.; Mirghafari, R.; Akbari, H. Trend analysis of hydrological and water quality variables to detect anthropogenic effects and climate variability on a river basin scale: A case study of Iran. *J. Hydro-Environ. Res.* **2021**, *34*, 11–23. [CrossRef]
5. Zuzani, P.; Ngongondo, C.; Mwale, F.; Willems, P. Examining trends of hydro-meteorological extremes in the Shire River Basin in Malawi. *Phys. Chem. Earth A B C* **2019**, *112*, 91–102. [CrossRef]
6. Bui, H.X.; Li, Y.-X.; Maloney, E.D.; Kim, J.-E.; Lee, S.-S.; Yu, J.-Y. Emergence of Madden-Julian oscillation precipitation and wind amplitude changes in a warming climate. *Npj Clim. Atmos. Sci.* **2023**, *6*, 22. [CrossRef]
7. Zhang, Q.; Zhao, Y.; Li, Y. Research progress and prospect on causes and variation of drought events in China. *J. Meteorol.* **2020**, *78*, 22.
8. Zhang, X.; Xu, W. Diurnal Variations in Rainfall and Precipitation Asymmetry of Tropical Cyclones in the Northwest Pacific Region. *J. Clim.* **2021**, *34*, 5565–5582. [CrossRef]
9. Javed, A.; Cheng, V.Y.; Arhonditsis, G.B. Detection of spatial and temporal hydro-meteorological trends in Lake Michigan, Lake Huron and Georgian Bay. *Aquat. Ecosyst. Health Manag.* **2019**, *22*, 1–14. [CrossRef]
10. Gupta, N.; Gond, S.; Gupta, S.K. Spatiotemporal trend characteristics of rainfall and drought jeopardy over Bundelkhand Region, India. *Arab. J. Geosci.* **2022**, *15*, 1155. [CrossRef]
11. Ahmad, I.; Tang, D.; Wang, T.; Wang, M.; Wagan, B. Precipitation trends over time using Mann-Kendall and spearman's rho tests in swat river basin, Pakistan. *Adv. Meteorol.* **2015**, *2015*, 431860. [CrossRef]
12. Alifujiang, Y.; Abuduwaili, J.; Ge, Y. Trend Analysis of Annual and Seasonal River Runoff by Using Innovative Trend Analysis with Significant Test. *Water* **2021**, *13*, 95. [CrossRef]
13. Hamed, K.H.; Rao, A.R. A modified Mann-Kendall trend test for autocorrelated data. *J. Hydrol.* **1998**, *204*, 182–196. [CrossRef]
14. Sa'adi, Z.; Shahid, S.; Ismail, T.; Chung, E.-S.; Wang, X.-J. Trends analysis of rainfall and rainfall extremes in Sarawak, Malaysia using modified Mann–Kendall test. *Meteorol. Atmos. Phys.* **2019**, *131*, 263–277. [CrossRef]
15. Mondal, A.; Kundu, S.; Mukhopadhyay, A. Rainfall trend analysis by Mann-Kendall test: A case study of north-eastern part of Cuttack district, Orissa. *Int. J. Geol. Earth Environ. Sci.* **2012**, *2*, 70–78.
16. Umar, D.A.; Ramli, M.F.; Aris, A.Z.; Wan, N.; Basiru, H.A. Runoff irregularities, trends, and variations in tropical semi-arid river catchment. *J. Hydrol. Reg. Stud.* **2018**, *19*, 335–348. [CrossRef]
17. Brigadier, L.; Bwalya, K.; Nkolola, N.B.; Chilekana, N. Quantifying long-term variability of precipitation and temperature over Zambia. *J. Atmos. Sol. Terr. Phys.* **2020**, *198*, 105201.
18. Deng, P.; Zhang, M.; Hu, Q.; Wang, L.; Bing, J. Pattern of spatio-temporal variability of extreme precipitation and flood-waterlogging process in Hanjiang River basin. *Atmos. Res.* **2022**, *276*, 106258. [CrossRef]
19. De Oliveira, R.G.; Valle Júnior, L.C.G.; Da Silva, J.B.; Espíndola, D.A.L.F.; Lopes, R.D.; Nogueira, J.S.; Curado, L.F.A.; Rodrigues, T.R. Temporal trend changes in reference evapotranspiration contrasting different land uses in southern Amazon basin. *Agric. Water Manag.* **2021**, *250*, 106815. [CrossRef]
20. Bouizrou, I.; Aqnouy, M.; Bouadila, A. Spatio-temporal analysis of trends and variability in precipitation across Morocco: Comparative analysis of recent and old non-parametric methods. *J. Afr. Earth Sci.* **2022**, *196*, 104691. [CrossRef]
21. Hu, J.; Li, P.; Zhao, G.; Mu, X.; Hoermann, G.; Gao, P.; Sun, W.; Zhang, L. Effects of climate variability and anthropogenic factors on sediment load reduction in the Weihe River basin, China. *Hydrol. Process.* **2022**, *36*, e14562. [CrossRef]
22. Sharma, V.; Nicholson, C.M.; Bergantino, A.; Irmak, S.; Peck, D. Temporal Trend Analysis of Meteorological Variables and Reference Evapotranspiration in the Inter-Mountain Region of Wyoming. *Water* **2020**, *12*, 2159. [CrossRef]
23. Gulakhmadov, A.; Chen, X.; Gulahmadov, N.; Liu, T.; Gulakhmadov, M. Long-Term Hydro-Climatic Trends in the Mountainous Kofarnihon River Basin in Central Asia. *Water* **2020**, *12*, 2140. [CrossRef]
24. Grinsted, A.; Moore, J.C.; Jevrejeva, S. Application of the cross wavelet transform and wavelet coherence to geophysical time series. *Nonlinear Process. Geophys.* **2004**, *11*, 561–566. [CrossRef]
25. Sun, W.; Cheng, B. Application of cross wavelet transform to analysis on regional climate variations. *J. Appl. Meteorol. Sci.* **2008**, *19*, 479–487.
26. Yu, D.; Zhang, R.; Hong, M.; Liu, K. Correlation analysis between the West Pacific subtropical high and the East Asian summer monsoon system based on cross wavelet and wavelet coherence. *J. Nanjing Inst. Meteorol.* **2008**, *30*, 755–769.
27. Wang, G.; Jiang, D.; Wang, Y.; Yu, Z. Characteristics of climate change in the Lake Dongting Basin (1961–2003). *J. Lake Sci.* **2006**, *18*, 470–475.

28. Xu, W.; Ge, D.; Li, N. Characteristics of Precipitation Variation in the Dongting Lake Basin during 1961–2011. *Wetl. Sci.* **2016**, *14*, 108–112.
29. Li, J.; Huang, S.; Li, J. Spatial-temporal characteristics of temperature in the Lake Dongting Basin from 1960 to 2008, Water Systems and Sustainable Management of water Resources. In Proceedings of the 7th China Water Forum, Beijing, China, 19–20 September 2009; pp. 82–88.
30. Zhang, M.; Zeng, Y.; Qi, Y. Analyzing spatio-temporal variations of evapotranspiration in Dongting Lake Basin during 2000–2014 based on MOD16. *Trans. Chin. Soc. Agric. Eng.* **2018**, *34*, 9.
31. Moghimi, M.M.; Zarei, A.R.; Mahmoudi, M.R. Seasonal drought forecasting in arid regions, using different time series models and RDI index. *J. Water Clim. Chang.* **2019**, *11*, 633–654. [CrossRef]
32. Chen, C.; Gan, R.; Feng, D.; Yang, F.; Zuo, Q. Quantifying the contribution of SWAT modeling and CMIP6 inputting to streamflow prediction uncertainty under climate change. *J. Clean. Prod.* **2022**, *364*, 132675. [CrossRef]
33. Zhang, J.; Li, Z.; Zhang, X.; Wu, P. Precipitation: Spatio-temporal Distribution Characteristics and Trend Change in Hunan Province from 1960 to 2005. *J. Hydrol.* **2009**, *29*, 73–78.
34. Song, C.; Fan, C.; Zhu, J.; Wang, J.; Sheng, Y.; Liu, K.; Chen, T.; Zhan, P.; Luo, S.; Yuan, C. A comprehensive geospatial database of nearly 100 000 reservoirs in China. *Earth Syst. Sci. Data* **2022**, *14*, 4017–4034. [CrossRef]
35. Mann, H.B. Nonparametric tests against trend. *Econom. J. Econom. Soc.* **1945**, *13*, 245–259. [CrossRef]
36. Kendall, M.G. *Rank Correlation Methods*; Griffin: New York, NY, USA, 1948.
37. Pettitt, A.N. A non-parametric approach to the change-point problem. *J. R. Stat. Soc. Ser. C Appl. Stat.* **1979**, *28*, 126–135. [CrossRef]
38. Gerstengarbe, F.W.; Werner, P.C. Estimation of the beginning and end of recurrent events within a climate regime. *Vis. Books* **1999**, *11*, 97–107. [CrossRef]
39. Feidas, H. Trend analysis of air temperature time series in Greece and their relationship with circulation using surface and satellite data: Recent trends and an update to 2013. *Theor. Appl. Climatol.* **2016**, *129*, 1383–1406. [CrossRef]
40. Sen, P.K. Estimates of the Regression Coefficient Based on Kendall's Tau. *J. Am. Stat. Assoc.* **1968**, *63*, 1379–1389. [CrossRef]
41. Torrence, C.; Compo, G.P. A practical guide to wavelet analysis. *Bull. Am. Meteorol. Soc.* **1998**, *79*, 61–78. [CrossRef]
42. Carey, S.K.; Tetzlaff, D.; Buttle, J.; Laudon, H.; McDonnell, J.; McGuire, K.; Seibert, J.; Soulsby, C.; Shanley, J. Use of color maps and wavelet coherence to discern seasonal and interannual climate influences on streamflow variability in northern catchments. *Water Resour. Res.* **2013**, *49*, 6194–6207. [CrossRef]
43. Juez, C.; Nadal-Romero, E. Long-term temporal structure of catchment sediment response to precipitation in a humid mountain badland area. *J. Hydrol.* **2021**, *597*, 125723. [CrossRef]
44. Juez, C.; Garijo, N.; Hassan, M.; Nadal-Romero, E. Intraseasonal-to-Interannual analysis of discharge and suspended sediment concentration time-series of the upper changjiang (Yangtze river). *Water Resour. Res.* **2021**, *57*, e2020WR029457. [CrossRef]
45. Grossmann, A.; Morlet, J. Decomposition of Hardy functions into square integrable wavelets of constant shape. *SIAM J. Math. Anal.* **1984**, *15*, 723–736. [CrossRef]
46. Panagiotopoulou, A.; Anastassopoulos, V. Super-resolution image reconstruction employing Kriging interpolation technique. In Proceedings of the 2007 14th International Workshop on Systems, Signals and Image Processing and 6th EURASIP Conference focused on Speech and Image Processing, Multimedia Communications and Services, Maribor, Slovenia, 27–30 June 2007; pp. 144–147.
47. Liu, Z.; Liu, Y.; Hao, Y. Multi-time scale cross-wavelet transformation between runoff and climate factors in the upstream of Heihe River. *Arid. Land Geogr.* **2014**, *37*, 1137–1146.
48. Liu, J.; Fu, G.; Song, X.; Charles, S.P.; Zhang, Y.; Han, D.; Wang, S. Stable isotopic compositions in Australian precipitation. *J. Geophys. Res.* **2010**, *115*, D23307. [CrossRef]
49. Zhou, H. *Impact of Climate Change on Water Resources in Dongting Lake Basin*; Hunan Normal University: Changsha, China, 2016.
50. Xu, K.; Milliman, J.D. Seasonal variations of sediment discharge from the Yangtze River before and after impoundment of the Three Gorges Dam. *Geomorphology* **2009**, *104*, 276–283. [CrossRef]
51. Valdivielso, S.; Hassanzadeh, A.; Vázquez-Sué, E.; Custodio, E.; Criollo, R. Spatial distribution of meteorological factors controlling stable isotopes in precipitation in Northern Chile. *J. Hydrol.* **2022**, *605*, 127–380. [CrossRef]
52. Palazzi, E.; Filippi, L.; von Hardenberg, J. Insights into elevation-dependent warming in the Tibetan Plateau-Himalayas from CMIP5 model simulations. *Clim. Dyn.* **2017**, *48*, 3991–4008. [CrossRef]
53. Li, S.; Jiang, C.; Ma, Y.; Long, Y.; Wu, R.; Zhu, Q.; Li, D.; Li, C.; Ning, Z. Adaptation Analysis in IMERG Precipitation Estimation for the Dongting Lake Basin, China. *Atmosphere* **2022**, *13*, 1735. [CrossRef]
54. Gohain, K.J.; Mohammad, P.; Goswami, A. Assessing the impact of land use land cover changes on land surface temperature over Pune city, India. *Quat. Int.* **2021**, *575*, 259–269. [CrossRef]

55. Gong, C.; Dan, L.; Yong, W.; Tingting, K. Water Area Change of Dongting Lake Based on Landsat Data and ItsAffecting Factors Analysis. *J. Irrig. Drain.* **2015**, *34*, 252–255.
56. Wang, R.; Peng, W.; Liu, X.; Jiang, C.; Wu, W.; Chen, X. Characteristics of Runoff Variations and Attribution Analysis in the Poyang Lake Basin over the Past 55 Years. *Sustainability* **2020**, *12*, 944. [CrossRef]